

Eccentric Phase Transition from Thermalization to Many Body Localization in Long-Range Spin Systems using Floquet Engineering

Mahbub Rahaman,¹ Takashi Mori,² and Analabha Roy¹

¹*Department of Physics, The University of Burdwan, Golapbag, Bardhaman - 713 104, India*
²*RIKEN CEMS, 2-1 Hirosawa, Wako, Saitama, 351-0198, Japan*

Many-body localization is a quantum phenomenon where a quantum system retains its initial state under certain resonance conditions, $J_0(\eta)$ which prevents the system to undergo thermalization. We have validated many-body localization for spin systems driven by transverse field and parametrized it by the Inverse Participation ratio(IPR) of Floquet modes. Long-range power-law dependence *i.e.* $J_{ij} = 1/|i - j|^\beta$ has been applied and we investigated for $\beta = \infty$ for short-range Transverse Field Ising Model and for $\beta = 0$ long-range Lipkin Meshkov-Glick (LMG) model is explored both at low and high drive frequencies. At the localization point Ising model exhibit full localisation at high frequency though at low-frequency localization persists. For the long-range case, at the system localization point, LMG shows localization at high frequency though at smaller frequency localization breaks down with inverse system size law. Similar behaviour is found in LMG at the phase-space continuum limit where at low-frequency chaos emerges and at the higher frequency it is regular. IPR for LMG is evolved by an adiabatic increase in drive frequencies; the IPR rises sharply thereby introducing a phase transition which manifests a future protocol for the MBL engine.

NEED TO PROOFREAD THIS. WILL DO AT THE END.

Periodically driven Many Body Systems can experience dynamical freezing (DMF) when a dynamical hysteresis stops observables from reaching their diagonal averaged values and thermalizing to infinite temperature [1–3]. Under certain resonance conditions in the drive parameters, DMF can cause the response to ‘freeze’ completely to its initial value at all times. This has been demonstrated via the Jordan-Wigner (JW) transformation in the driven TFIM with nearest neighbour interactions [4] and is shown to be protected when translational invariance is explicitly broken (say, by disorder) [5, 6].

We have a hunch that this symmetry is preserved against the loss of other symmetries such as Long-range systems for which the JW transformation results in non-localities. To prove this, we introduce a long-range power-law dependence in the TFIM, where the exchange $J_{ij} \sim 1/|i - j|^\beta$; for $\beta = \infty$ [7–9], we recover the short-range TFIM and freezing at resonant drive parameters. When $\beta = 0$, taking $N \rightarrow \infty$ allows us to describe the exact dynamics by the periodically driven Lipkin-Meshkov-Glick (LMG) model.

Now, we compare the degree of localization of the quasi-stationary Floquet modes in both cases. In order to do so, we look at the Inverse Participation Ratio (IPR) of the Floquet modes in the representation given by the eigenstates of the symmetry-breaking field. The Inverse Participation Ratio (IPR) [10] a parameter is a useful tool for defending the many-body localization of a quantum system. For a many-body localized system, IPR is unity and it varies as the inverse of the system size when it is fully distributed [11].

In the first section of this paper, we presented a brief overview of essential theoretical frameworks. The Ising Model driven by a transverse periodic field which breaks symmetry is presented next in section II. Rotating Wave Approximation (RWA) [12], where only the slowest ro-

tating terms in the Fourier expansion of the Hamiltonian in a frame co-rotating with symmetry breaking drive field are retained, is used to make a close approximation of the Ising Hamiltonian, and higher-order corrections are obtained also. We have applied the Floquet theory of a periodically driven system and obtained Floquet modes to get the IPR of the Floquet modes. It is used to probe the system dynamics in the high and low-frequency domains. In section III we introduce LMG model as a paradigmatic spin model for long-range spin-spin interaction. We formulated the system Hamiltonian which governs it at a continuum limit and also simplified it using RWA to find Floquet-IPR for low and high-frequency regions of operation. In section IV we have contrasted the classical Lipkin model driven with both at a higher frequency and sufficient lower frequency for phase-space and Hushimi Q-functions analysis. In section V we have discussed the system dynamics driven by adiabatically increased drive frequency from low to high limit thereby we discover a phase transition at the system localization resonance point. Finally, we conclude and discuss the outlook.

I. BACKGROUND

PROOFREADING THIS NOW.

If a generic closed isolated interacting quantum many-body system is prepared in a state that is far enough from equilibrium, the ensuing dynamics is expected to reproduce the statistical behaviour of a microcanonical ensemble. The long-term averages of observables, resolved in the framework of the Eigenstate Thermalization Hypothesis (ETH)[13, 14]. Let the system be described by a Hamiltonian \hat{H} , and be populated at an initial state $|\Psi_0\rangle$ at $t = 0$. The expectation value of an observable \hat{O} can be obtained at all times by solving the Heisenberg

equation of motion

$$\frac{d}{dt} \langle \hat{O}(t) \rangle = i \left\langle [\hat{H}, \hat{O}(t)] \right\rangle. \quad (1)$$

The solution can be written as

$$\begin{aligned} \langle \hat{O}(t) \rangle &= \left\langle e^{i\hat{H}t} \hat{O} e^{-i\hat{H}t} \right\rangle \\ &= \sum_{ij} e^{-i(e_i - e_j)t} O_{ij} \langle \Psi_0 | e_i \rangle \langle e_j | \Psi_0 \rangle \end{aligned}$$

Here, the reduced Planck's constant \hbar has been set to unity. Furthermore, the eigendecomposition of \hat{H} yields eigenvalues e_i and corresponding eigenvectors $|e_i\rangle$, indexed by a count i , and are expected to be non-degenerate. Also, the matrix element $O_{ij} \equiv \langle e_i | \hat{O} | e_j \rangle$. If the long-time average of an object is expressed by an overline, then

$$\begin{aligned} \overline{\langle \hat{O}(t) \rangle} &= \sum_{ij} \overline{e^{-i(e_i - e_j)t}} O_{ij} \langle \Psi_0 | e_i \rangle \langle e_j | \Psi_0 \rangle. \\ &\approx \sum_i O_{ii} |\langle e_i | \Psi_0 \rangle|^2 + \mathcal{O}(e^{-S/2}). \end{aligned} \quad (2)$$

In equation 2 the entropy S is a monotonic function of the initial energy $E_0 = \langle \Psi_0 | \hat{H} | \Psi_0 \rangle$ that arises from the Srednicki ansatz [15, 16] concerning the nature of the matrix elements O_{ij} , *viz.*

$$O_{ij} \approx O_{ii} \delta_{ij} + e^{-S/2} \mathcal{R}_{ij},$$

with nearly random off-diagonal contributions \mathcal{R}_{ij} . This ansatz, together with the fact that, at sufficiently long times, $e^{-i(e_i - e_j)t} \rightarrow \delta_{ij}$, justifies neglecting the second term in the RHS of equation 2.

Next, the 'typicality' conjecture proposes that the resolution of $|\Psi_0\rangle$ in the eigenbasis of the Hamiltonian is 'typical', *i.e.*, the dominant modes have energies that lie in a small but nonzero neighbourhood δE of E_0 , which is assumed to be significantly greater than the ground state energy. When this conjecture is evoked, the *diagonal average* in equation 2 can be simplified further to yield

$$\overline{\langle \hat{O}(t) \rangle} \approx \sum_{|e_k\rangle \in \mathcal{S}(E_0, \delta E)} O_{kk} |\langle e_k | \Psi_0 \rangle|^2 \quad (3)$$

Here, the summed sector consists of the states $|e_k\rangle$ whose energies lie in a δE -neighbourhood of E_0 , *i.e.*

$$\mathcal{S}(E_0, \delta E) = \left\{ |e_k\rangle \ni E_0 - \frac{\delta E}{2} \leq e_k \leq E_0 + \frac{\delta E}{2} \right\}$$

The final proposition is that the RHS of equation 3 can be represented by an integral over a continuous energy

measure dE , such that

$$\begin{aligned} \overline{\langle \hat{O}(t) \rangle} &= \sum_{|e_k\rangle \in \mathcal{S}(E_0, \delta E)} O_{kk} |\langle e_k | \Psi_0 \rangle|^2 \\ &\approx \frac{1}{|\mathcal{S}(E_0, \delta E)|} \int O(E) g(E) dE, \end{aligned} \quad (4)$$

where $O(E)$ is a sufficiently smooth function that represents O_{kk} in the summed sector $\mathcal{S}(E_0, \delta E)$, $g(E)$ is the density of states at E , and $|\mathcal{S}(E_0, \delta E)| = \int g(E) dE$ denotes the cardinality of the set $\mathcal{S}(E_0, \delta E)$. Here, the integrals are performed in the range $D(E_0) = [E_0 - \frac{\delta E}{2}, E_0 + \frac{\delta E}{2}]$. With this proposition, the Lagrange Integral Mean Value Theorem (see, for instance [17]) may be evoked, where there exists a value $\bar{E} \in D(E_0)$ such that

$$\int O(E) g(E) dE = O(\bar{E}) \int g(E) dE.$$

Substituting this result into eqn 4 yields

$$\overline{\langle \hat{O}(t) \rangle} \approx O(\bar{E}) \quad (5)$$

If $\delta E \ll E_0$, the quantity $O(\bar{E})$ in eqn 5 should be close to an average of O_{kk} over the states in $\mathcal{S}(E_0, \delta E)$. Thus,

$$\overline{\langle \hat{O}(t) \rangle} \approx O(\bar{E}) \approx \frac{1}{|\mathcal{S}(E_0, \delta E)|} \sum_{|e_k\rangle \in \mathcal{S}(E_0, \delta E)} O_{kk}. \quad (6)$$

The RHS of equation 6 corresponds to the standard microcanonical average in statistical mechanics. This is the *Eigenstate Thermalization Hypothesis* (ETH), first proposed by Deutsch [18] and presented in this form by Srednicki [19]. The long-term behaviour of a system obeying ETH is independent of the initial condition $|\Psi_0\rangle$ as a direct result of equation 6. Despite the lack of ergodicity in the underlying Heisenberg dynamics, the system can start from any typical state at $t = 0$ and exhibit universal thermal behaviour.

If the many body system is described by a time-periodic Hamiltonian $\hat{H}(t)$ with a very small time period T , we can expect the system to behave similarly to the time-independent case discussed above, except that it will thermalize at infinite temperature. If the system is strobed at integer multiples of the time period T , *Floquet Theory* allows us to obtain *quasi-stationary states* (stationary only at integer multiples of time period T) from the eigendecomposition of the Floquet Hamiltonian $\hat{H}_F \equiv \hat{H}(T) - i \frac{\partial}{\partial t}|_T$ (see, for instance, [20, 21] and references therein). In that case, the ETH introduced in equations 2 and 3 may be modified with $e_i, |e_i\rangle$ replaced by the eigendecomposition of \hat{H}_F , given by $\Omega_i, |\phi_i\rangle$, provided that T is sufficiently small to ignore the Floquet

micromotions between two successive periods. Thus,

$$\begin{aligned} \overline{\langle \hat{O}(nT) \rangle} &\approx \sum_{ij} \overline{e^{-i(\Omega_i - \Omega_j)nT}} O_{ij} \langle \Psi_0 | \phi_i \rangle \langle \phi_j | \Psi_0 \rangle. \\ &\approx \sum_i O_{ii} \left| \langle \phi_i | \Psi_0 \rangle \right|^2 \approx \sum_{|\phi_k| \in S'(\Omega_0, \delta\Omega)} O_{kk} |\langle \phi_k | \Psi_0 \rangle|^2, \end{aligned} \quad (7)$$

where the new set

$$S'(\Omega_0, \delta\Omega) = \left\{ |\phi_k\rangle \ni \Omega_0 - \frac{\delta\Omega}{2} \leq \Omega_k \leq \Omega_0 + \frac{\delta\Omega}{2} \right\},$$

and the quantities $\Omega_0, \delta\Omega$ are obtained by adding integer multiples of $\omega = 2\pi/T$ to $E_0, \delta E$ to make them lie within a Floquet photon *viz.* an interval of width ω . Even in this limit, drive parameters like amplitude, frequency, and duty-cycle strongly affect the ϕ_i s. Thus, they can be engineered to make O_{kk} in equation 7 weakly dependent on $|\phi_k\rangle$, but the initial quasi energy Ω_0 heavily dependent. In particular, the functional derivative δO_{kk} $\delta |\phi_k\rangle$ can be made arbitrarily large. The continuum limit in eqn 4 can no longer be justified, suppressing thermalization dynamically. Thus, Floquet Engineering of quasienergies can produce Dynamical Many Body Localization (DMBL), where the system fails to reach thermal equilibrium and remains localised near its initial state even at large times. This paradigm is similar to MBL, where disorder, locality, and integrability cause athermality. Localization can occur regardless of disorder, locality of observables, or system integrability, all of which have been studied for MBL onset [22–24]. However, DMBL has been shown in integrable systems where specific drive parameters can produce additional approximate Noether charges that cause dynamical localization [6].

A paradigmatic example of an integrable system where DMBL occurs is the driven Transverse Field Ising model (TFIM) in one dimension [25]. The Hamiltonian is given by

$$\hat{H}(t) = \hat{H}_0 + h_z(t) \hat{H}_1 \quad (8)$$

$$\hat{H}_0 = -\frac{1}{2} \sum_{i=1}^N \sigma_i^x \sigma_{i+1}^x \quad (9)$$

$$\hat{H}_1 = -\frac{1}{2} \sum_{i=1}^N \sigma_i^z. \quad (10)$$

Here, the undriven Hamiltonian \hat{H}_0 consists of nearest-neighbour interactions between N spin-1/2 particles on a one-dimensional lattice. The transverse field is given by \hat{H}_1 , and is being modulated by a time-periodic and harmonic signal $h_z(t) = h_0 + h \cos \omega t$, yielding a time period $T = 2\pi/\omega$ with amplitude h , drive frequency ω , and d.c. field h_0 . This Hamiltonian can be readily transformed into a spinless pseudo-fermionic system via the

Jordan-Wigner transformation. Written in momentum space spanned by spinors $\psi_k = (c_{-k}, c_k^\dagger)^T$ of fermions at momentum k created (annihilated) by operators c_k^\dagger (c_k). This yields an effective Hamiltonian [4]

$$H(t) = \sum_{(k, -k)-\text{pairs}} \psi_k^\dagger \left[\left(f_k - h_z(t) \right) \tau_z + \tau_x \Delta_k \right] \psi_k \quad (11)$$

with $f_k = J \cos k$, $\Delta_k = J \sin k$, τ_{xyz} are the three Pauli Matrices, and the sum is over distinct $(k, -k)$ Cooper Pairs. Now, we transform to the rotated frame via the unitary transformation operator $U(t) = \prod_k U_k(t)$, where $U_k(t) = \exp \left\{ \left[\frac{i\hbar}{\omega} \sin \omega t \right] \tau_z \right\}$. This yields the transformed Hamiltonian

$$\begin{aligned} H'(t) = \sum_{(k, -k)-\text{pairs}} \psi_k^\dagger & \left[\tau_z f_k + \tau_x \cos (\eta \sin \omega t) \right. \\ & \left. + \tau_y \cos (\eta \sin \omega t) \right] \psi_k, \end{aligned}$$

where we defined $\eta = 2h/\omega$. Using the Jacobi-Anger formula $e^{i\eta \sin \omega t} = \sum_{n=-\infty}^{\infty} J_n(\eta) e^{in\omega t}$, the transformed Hamiltonian simplifies to

$$\begin{aligned} H'(t) = \sum_{(k, -k)-\text{pairs}} \psi_k^\dagger & \left[\tau_z f_k + 2\tau_x \Delta_k \sum_{n \geq 0} J_{2n}(\eta) \cos (2n\omega t) \right. \\ & \left. - 2\tau_y \Delta_k \sum_{n \geq 0} J_{2n+1}(\eta) \sin \{(2n+1)\omega t\} \right] \psi_k, \end{aligned} \quad (12)$$

Now, for large $\omega \gg f_k$, we can approximate $H'(t)$ by its long-time average $\overline{H'(t)}$, leaving behind only the non-oscillating modes, a *Rotated Wave Approximation* that yields an effective time-independent Hamiltonian,

$$H^{RWA} = \sum_{(k, -k)-\text{pairs}} \psi_k^\dagger \left[f_k \tau_z + 2J_0(\eta) \Delta_k \tau_x \right] \psi_k, \quad (13)$$

Clearly, if we engineer drive parameters such that η lies on a root of $J_0(\eta)$, a straightforward case of Floquet Engineering, then the fermion number (THIS PART STILL NEEDS WORK) becomes an approximately conserved quantity at this resonance. Thus, it is possible to directly control H^{RWA} and induce a complete freezing of otherwise responsive observables. That this leads to a spectacular breakdown of ETH can be readily demonstrated by ... NOW CONTEXUALIZE THIS WRT THE DREK ABOUT FUNCTIONAL DERIVATIVES...

The extent to which a particular (quasi) stationary state is localized (or frozen) in a physically meaningful representation can be quantified by the *Inverse Participation Ratio* (IPR). In the position representation, the IPR for a state $|\psi\rangle$ [26–29] is defined as

$$\phi_{IPR} \equiv \int d\mathbf{x} |\langle \mathbf{x} | \psi \rangle|^4$$

This definition can be generalized to the IPR of a state $|\phi\rangle$ in a representation given by complete orthonormal basis $|m\rangle$ as

$$\phi_{IPR} \equiv \sum_m |\langle m|\psi\rangle|^4. \quad (14)$$

The smallest value of the IPR corresponds to a fully delocalized state, $\psi(x) = 1/\sqrt{N}$ for a system of size N [29, 30]. Values of the IPR close to unity correspond to localized states [31]. For a periodically driven system, we look at the IPR of the quasi-stationary Floquet modes at $t = T$, where $t = 2\pi/\omega$ for drive frequency ω . In the TFIM model, equation 13 indicates that, at resonance, when $J_0(\eta) = 0$, the Floquet modes are approximately given by the fermionic Fock states, which have a trivially unit IPR in the representation of the eigenmodes of the transverse field \hat{H}_1 in equation 8.

For the TFIM case, a particular Floquet mode can be decomposed into a direct product of cooper-pair states as $|\phi\rangle = \prod_{k,-k} |\phi_k^n\rangle$. In the RWA limit and at resonance, $|\phi_k^n\rangle$ has values of $|0\rangle, |k, -k\rangle$ for two values of $n = 0, 1$ respectively. We define the reduced IPR of $|\phi_k^n\rangle \forall k$ to be

$$\phi_{IPR}^{(n)}(k) = |\langle 0|\phi_k^n\rangle|^4 + |\langle +k, -k|\phi_k^n\rangle|^4, \quad (15)$$

where $n = 0, 1$. In the RWA limit and at resonance, this quantity is unity, indicating very low participation and the onset of freezing. Figure 1 shows results from numerically simulating the TFIM dynamics. The reduced IPR for a particular Floquet mode was obtained by simulating the exact Heisenberg dynamics over a single time period of the drive, and plotted as a function of momentum k for different η 's. At resonance, when η lies at the root of the Bessel function $J_0(\eta)$, the IPR is exactly unity for all momenta. Outside this resonance, the IPR is unity only for some momenta because the effective Hamiltonian is perfect diagonal at $k \in \{-\pi, 0, \pi\}$ as can be seen in the cross-sectional plots of figure 1. Away from the resonance point, IPR is less than unity but as TFIM is integrable spin model, it does not follow thermalization maintaining positive value. However, at low frequencies, when RWA fails due to unavailability of zero offdiagonal terms in the effective transformed Hamiltonian (in matrix representation) and no integrability breaking terms to counteract the off diagonal terms, the IPR remains quite high ($IPR \sim 0.5$) even at resonance point as can be seen figure 2. At low frequency, this is valid for all momentum and parameter η , see figure 3.

Because the dependence of observable expectations on the eigenstates is always fairly strong for integrable systems like the TFIM, such systems will never exhibit any kind of thermal behaviour unless integrability breaking terms are included. As a result, it is not physically meaningful to refer to this as "Many Body Localization," because the parameter space lacks a region where ETH holds to contrast with this state. The type of Floquet Engineering described above, on the other hand, can be easily applied to a broad class of nonintegrable systems

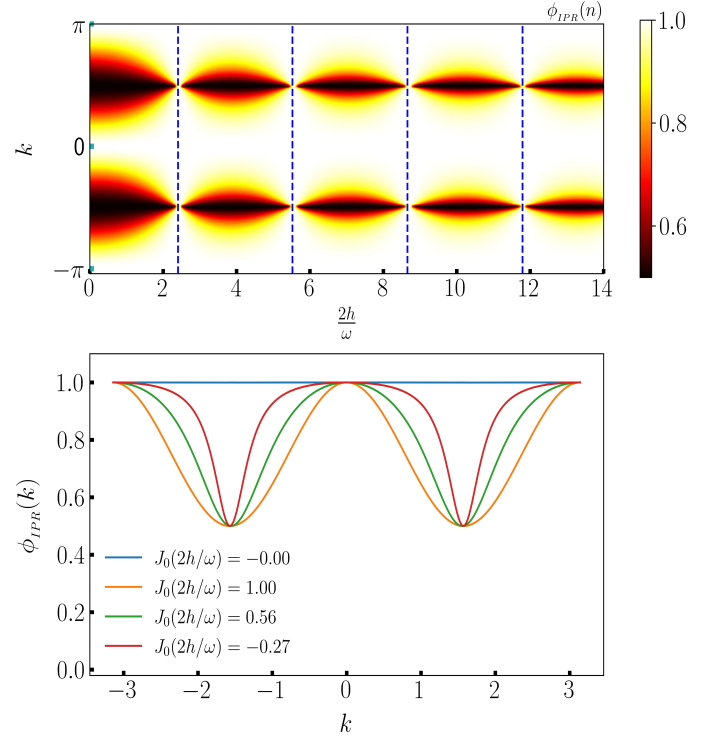


FIG. 1. The plots above are for the exact dynamics of the TFIM in Fermionic representation for size $N = 100$, with the reduced IPR (defined in equation 15) plotted for the entire Brillouin zone for a few drive amplitudes. The frequency is set to $\omega = 90$ and the IPR of one of the two Floquet modes are plotted at time $t = T$ for four different chosen amplitudes. The exact result is consistent with the RWA approximation. When $J_0(2h/\omega) = 0$, the RWA Hamiltonian vanishes, yielding an IPR of unity. At other points, the IPR is unity only when $k = \pm\pi$ (since $\Delta_k = 0$) and $k = 0$ (since $f_k = 0$ and the Hamiltonian for each $k \sim \sigma_x$); other than that, there is freezing due to the ensuing dynamics.

where ETH is expected to hold in certain regions. Long-range spin systems, in particular, where the exchange energies between far-off spins are taken into account in the model Hamiltonian, are good candidates because they are known to thermalize when driven with low frequencies [32].

II. LIPKIN MESHKOV GLICK MODEL: LONG RANGE INTERACTION

PROOFREAD FROM HERE!!!

FROM HERE ON OUT, PLZ USE THE PHYSICS LATEX PACKAGE!!!

Consider the Hamiltonian of the type

$$\hat{H}(t) = \hat{H}_0 + (h \cos(\omega t) + h_0) \hat{H}_1 \quad (16)$$

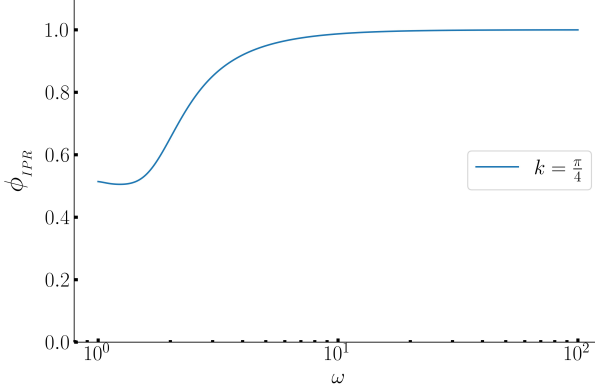


FIG. 2. IPR for TFIM is approximately 0.5 at lower frequency and 1 at higher frequency. The slow change in IPR from minimum to unity over a large frequency range indicates the absence of a mobility edge and, consequently, the absence of a phase transition. In addition, at the point of resonance at low frequency the system does not go ETH-thematization is indicated by the existence of a finite IPR.

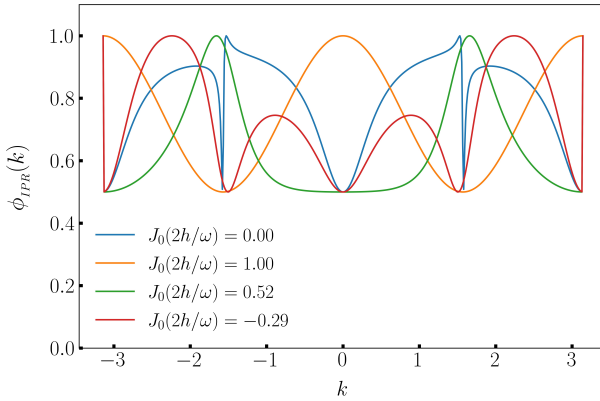


FIG. 3. A low-frequency regime $\omega = 2.0$ plot for IPR for Ising model at four different density points for system size $N = 500$. IPR localization persists nonetheless.

where

$$\begin{aligned}\hat{H}_0 &= \frac{1}{2} \sum_{ij} J_{ij} \hat{\sigma}_i^z \hat{\sigma}_j^z, \\ \hat{H}_1 &= \sum_i \hat{\sigma}_i^x.\end{aligned}$$

here,

$$J_{ij} = \frac{J_\alpha}{N^{1-\alpha}} \frac{1}{r_{ij}}.$$

Putting $\alpha = 0$ yields the Lipkin Meshkov Glick (LMG) model with all-to-all interaction, yielding $J_{ij} = J_0/N$.

We choose to maintain the extensivity of the interaction energy by enforcing the condition

$$\frac{J_0}{N} \sum_{i \neq j} 1 = \frac{J_0}{N} \frac{N(N-1)}{2} = 1$$

yielding the Kac-norm $J_0 = 2/(N-1)$. Here, we have N spin-1/2 particles in a 1-dimensional lattice, and i, j are site indices. The Hamiltonian in equation 16 commutes with P_{ij} with P_{ij} defined as $P_{ij} = \frac{1}{2}(1 + \vec{\sigma}_i \cdot \vec{\sigma}_j)$. In addition $[S^2, H] = 0$, therefore the S^2 is invariant of motion, where $S^2 = |\vec{S}|^2$ with \vec{S} defined as, $\vec{S} = S^x \hat{x} + S^y \hat{y} + S^z \hat{z} \equiv \frac{1}{2} \sum_i \vec{\sigma}_i$. We now choose to populate the system in a state whose measured value of S^2 is $\frac{N}{2} \left(\frac{N}{2} + 1 \right)$, in that case the dynamics remains invariant in the space spanned by the common eigen states of $P_{ij}, |S|^2$ and S_z , these are also eigenstates in the so-called TSS subspace [33]. Let the eigenvalues be s_n , and the eigen vectors be $|s_n\rangle$, where $s_n = -\frac{1}{2} + \frac{n}{N}$ and the index $n = 0(1)N$ has $N+1$ values. So, the dynamics is restricted to a $(N \times N)$ invariant subspace where the matrix elements are given by

$$\begin{aligned}(H_0)_{ij} &= -\frac{4}{N-1} s_i^2 \delta_{ij}, \\ (H_1)_{ij} &= \left[\sqrt{\frac{N}{2} \left(\frac{N}{2} + 1 \right) - N s_i (N s_{i+1})} \delta_{i+1,j} \right. \\ &\quad \left. + \sqrt{\frac{N}{2} \left(\frac{N}{2} + 1 \right) - N s_i (N s_{i-1})} \delta_{i-1,j} \right]\end{aligned}\quad (17)$$

Now we transform the Hamiltonian to the Rotated frame given by the transformation

$$\hat{U}(t) = \exp \left[i \frac{h}{\omega} \sin(\omega t) \hat{H}_1 \right] \quad (18)$$

Defining $\tau = \frac{h}{\omega} \sin \omega t$, we use the fact that $\hat{H}_1 = 2S^x$, and the identity

$$e^{i2\tau \hat{S}^x} \hat{S}^z e^{-i2\tau \hat{S}^x} = \hat{S}^z \cos(2\tau) + \hat{S}^y \sin(2\tau) \quad (19)$$

to simplify the transformed Hamiltonian, yielding

$$\begin{aligned}\tilde{H}(t) &= -\frac{1}{N-1} \left[(S^z)^2 (1 + \cos 4\tau) + (S^y)^2 (1 - \cos 4\tau) \right. \\ &\quad \left. + \{S^y, S^z\} \sin 4\tau \right] - 2h_0 S^x \quad (20)\end{aligned}$$

We define $\eta \equiv 4h/\omega$ and use the Jacobi-Anger formulae [34]

$$\cos(\eta \sin \omega t) = J_0(\eta) + 2 \sum_{n=1}^{\infty} J_{2n}(\eta) \cos(2n\omega t)$$

$$\sin(\eta \sin \omega t) = 2 \sum_{n=1}^{\infty} J_{2n-1}(\eta) \sin[(2n-1)\omega t]$$

to simplify the expression for $\tilde{H}(t)$. Finally, we assume that the drive frequency ω is large enough that all harmonic terms in the Hamiltonian can be averaged out over discernible time scales. This yields the Hamiltonian in the Rotated Wave Approximation (RWA) to be (ignoring constant terms in the addition)

$$\tilde{H}_{\text{RWA}} = \frac{(\hat{S}^x)^2}{N-1} - 2h_0\hat{S}^x - \frac{J_0(\eta)}{N-1} \left[(\hat{S}^z)^2 - (\hat{S}^y)^2 \right] \quad (21)$$

If the drive amplitude h is adjusted such that η lies at a root of $J_0(\eta)$ (the localization point), the RWA Hamiltonian is diagonal in the representation of the transverse field \hat{S}^x , yielding an IPR of unity in that representation, similar to the Ising case. Note however, that if the DC transverse field h_0 is set to 0, then, at the localization point, the RWA Hamiltonian $\tilde{H}_{\text{RWA}} \sim (\hat{S}^x)^2$, each of whose eigenvalues (given by $(\frac{N}{2} - m)^2$ where $m \in 0(1)N$, and $(\frac{N}{2} - m)$ are the eigenvalues of \hat{S}^x) are two-fold degenerate. This produces infinitely many (Floquet) eigenmodes in the degenerate subspace whose IPRs may not always be unity in the S^x representation. Thus, the absence of the DC field may produce delocalization in the Floquet states even at the localization points, and this necessitated the inclusion of a DC field h_0 in order to break the symmetry. Finally, note that not all values of the DC field h_0 remove all degeneracies in \tilde{H}_{RWA} . To see this, note that, at the localization point, the eigenvalues of \tilde{H}_{RWA} are given by

$$\text{Eigs}\left[\tilde{H}_{\text{RWA}}\right] = \frac{\left(\frac{N}{2} - m\right)^2}{N-1} - 2h_0\left(\frac{N}{2} - m\right) \quad (22)$$

In order to ensure that no degeneracies occur, we have to adjust h_0 to ensure that for any two integers $m_1, m_2 \leq N$ the condition following is always met,

$$\frac{\left(\frac{N}{2} - m_1\right)^2}{N-1} - 2h_0\left(\frac{N}{2} - m_1\right) \neq \frac{\left(\frac{N}{2} - m_2\right)^2}{N-1} - 2h_0\left(\frac{N}{2} - m_2\right) \quad (23)$$

If $N \gg 1$ (substantially large), then this condition can be met by assuring that $(1 - 2h_0)^{-1}$ is never an integer that is divisible by N . To ensure this in our numerical simulations we have kept h_0 at a small irrational value.

This result is tentatively supported by exact simulations, as can be seen in the plots below in FIG. 4. There, we show plots of the IPR of the Floquet mode $|\phi^n\rangle$ for

all n corresponding to eigenvalues of S^x for a fixed eigenvalue of $S^2 = N/2(N/2 + 1)$. The IPR is thus

$$\phi_{\text{IPR}}(n) = \sum_m |\langle m | \phi^n \rangle|^4 \quad (24)$$

where $|m\rangle$ is the m^{th} eigenstate of \hat{S}^x .

Now, we focus at numerical simulations for $H(t)$ via the IPR of the Floquet state in the representation of the transverse field i.e. the eigenstates of S^x . We kept $\omega = 90$ as a large enough value for RWA to hold, and $N = \mathcal{O}(10^2)$ which our standard computational resources will allow.

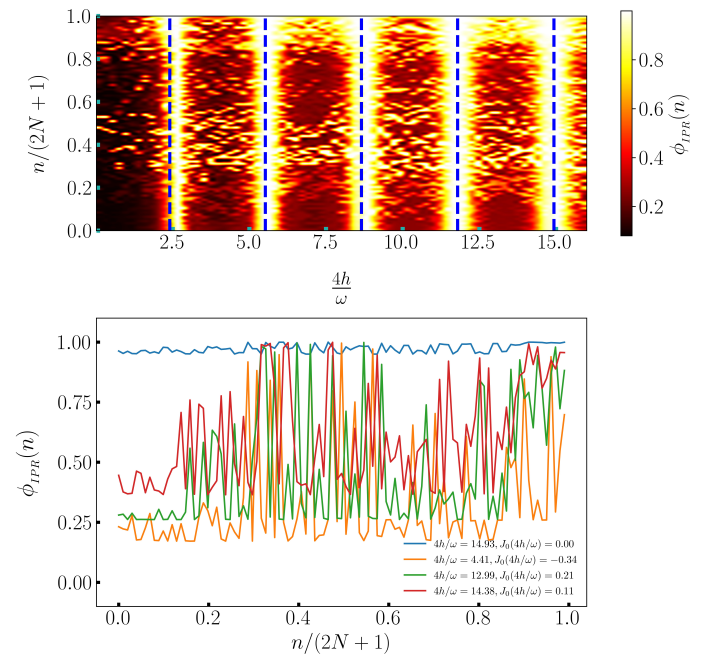


FIG. 4. The IPR for exact dynamics for spin model size $N \sim 30$. The upper panel shows a density plot of the IPR of Floquet modes for different parameter points corresponding to the ratio between strength and the frequency of the symmetry-breaking field which is the lowest root among Bessel's roots of the first kind and zeroth order $\frac{4h}{\omega}$. The dc part of the symmetry-breaking field is kept at a small irrational number to avoid the symmetry arising from degeneracy in Flqouet states. The IPR density is high at Bessel's first order roots, $J_0\left(\frac{4h}{\omega}\right) = 0$ for all the available floquet states. The lower panel shows the crossectional plot of IPR for four different floquet IPR density points. The point corresponding $J_0\left(\frac{4h}{\omega}\right) = 0$ has unity value for all states where points away from the roots have lower and high fluctuations.

The top panel has a density plot of the IPR of the Floquet states, with $\eta = 4h/\omega$ on the abscissa and the spin index $m/(2N+1)$ on the ordinate. The dashed vertical lines (blue) correspond to roots of $J_0(\eta)$. As can be seen, the IPR is essentially unity at large roots of $J_0(\eta)$, indicating complete Many Body localization. However, there is some departure from unity at the smallest root

of $J_0(\eta)$. This is due to the fact that at the smallest root of $J_0(\eta) \approx 2.405$, the amplitudes of the contributions of the higher order terms in the RW expansion, which are of $\mathcal{O}(J_n(\eta))$, are large enough to contribute to delocalization.

The bottom panel contains cross sections of the full IPR plot for selected values of η as indicated in the legend. When the drive amplitude h is adjusted to make $J_0(\eta) \neq 0$, the Floquet States are mixed, but not entirely thermal, since the IPR does not fall to $\mathcal{O}(N^{-1})$, indicat-

ing that localization persists to some extent always.

So, as long as there is an appropriate DC field, S^x is mostly conserved and H_F is mostly diagonal in the S^x representation at the freezing point. The small deviations from this conservation occur due to the role of higher order terms in the Fourier expansion of the Hamiltonian on the rotating basis that contribute additional time-periodic terms to the RWA Hamiltonian, as can be seen in FIG.II.

The full Hamiltonian for the LMG model on the rotated basis is

$$\begin{aligned} \tilde{H}^{RWA}(t) \sim & \frac{(\hat{S}^x)^2}{N-1} - 2h_0\hat{S}^x - \frac{J_0(\eta)}{N-1} \left[(\hat{S}^z)^2 - (\hat{S}^y)^2 \right] - \frac{2}{N-1} \sum_{n=1}^{\infty} J_{2n}(\eta) \left[(\hat{S}^z)^2 - (\hat{S}^y)^2 \right] \cos(2n\omega t) \\ & - \frac{2}{N-1} \sum_{n=1}^{\infty} J_{2n-1}(\eta) \{ \hat{S}^y, \hat{S}^z \} \sin[(2n-1)\omega t] \end{aligned} \quad (25)$$

IPR plots for precise dynamics describe that the freezing point at first (blue colour curve) Bessel's root of zeroth order of first kind is not enough for many-body localization in the top panel. This is because of the corresponding higher magnitude of other Bessel's roots of higher order. At higher localization points (shown in orange with dashes), many-body localization is most noticeable. Away from the point of localization, various curves, both green and red, represent how scattered the system is. RWA for zeroth order in the centre panel has a nearly identical pattern at places that are further away from localization points (green and red), but the curves for both higher and lower localization points have fully localised, which contradicts the precise conclusion found in the panel on top. In the bottom panel, RWA which has been corrected to the first order exhibits a similar curve structure with exact dynamics.

III. CLASSICAL LIPKIN DYNAMICS

In the classical(continuum) limit, $N \rightarrow \infty$, we can ignore the difference between adjacent values of s_i in equation 17, and the Hamiltonian per particle becomes $h(t) \equiv \frac{1}{N} H(t) = h + h_0 \cos(\omega t) h_1$, where

$$(h)_{ij} \approx -2s_i^2 \delta_{ij}, \\ H_0 \rightarrow -2s^2 \quad (26)$$

$$(h_1)_{ij} \approx \sqrt{1 - 4s_i^2} [\delta_{i+1,j} + \delta_{i-1,j}] \\ H_1 \rightarrow \sqrt{1 - 4s^2} \cos p, \quad (27)$$

In the continuum limit, the Lipkin system can be de-

scribed by p, q with corresponding Hamiltonian [35]:

$$H = -2q^2 - h(t) \sqrt{1 - 4q^2} \cos p, \quad (28)$$

which yields the Hamiltonian dynamical system

$$\begin{aligned} \frac{dq}{dt} &= h(t) \sqrt{1 - 4q^2} \sin p \\ \frac{dp}{dt} &= 4q \left[1 - \frac{h(t) \cos p}{\sqrt{1 - 4q^2}} \right] \end{aligned} \quad (29)$$

We solved Hamiltonian 28 using equations 29 to obtain position and momentum coordinates p, q and plotted in the Poincaré surface of section (PSOS) strobbed at each multiple of time period. A chaotic Poincare pattern is found for all small drive amplitude s.t. $A/J < 0.5$ and also a regular pattern emerges at for ratios $A/J \geq 0.5$ both at small drive frequency $\omega \sim 2.0$ [32].

But at a sufficient high-frequency regime, the system behaves differently. We have compared Poincare sections of the ensuing dynamics for $h(t) = h \cos \omega t$ for two cases, one for which $\omega = 2.5$ (smaller frequency and consequently small amplitude) and one at $\omega = 90.0$ (high frequency and corresponding high amplitude) at $J_0(4h/\omega) = 0$. These are compared with the Husimi Q-functions of the obtained Floquet States. The quantum phase space is described by the Spectral Average of the Husimi functions of all the Floquet modes $|\phi^n\rangle$ for the chosen value of S^2 , i.e. for a coherent state $|q, p\rangle$, we plot in FIG. 6.

$$H(q, p) \equiv \frac{1}{(2N+1)\pi} \sum_n \langle q, p | \phi^n \rangle \langle \phi^n | q, p \rangle$$

At small ω , where the classical plots are chaos dominated [36], and at large ω the sharp regular pattern proves localization in the Poincaré plot.

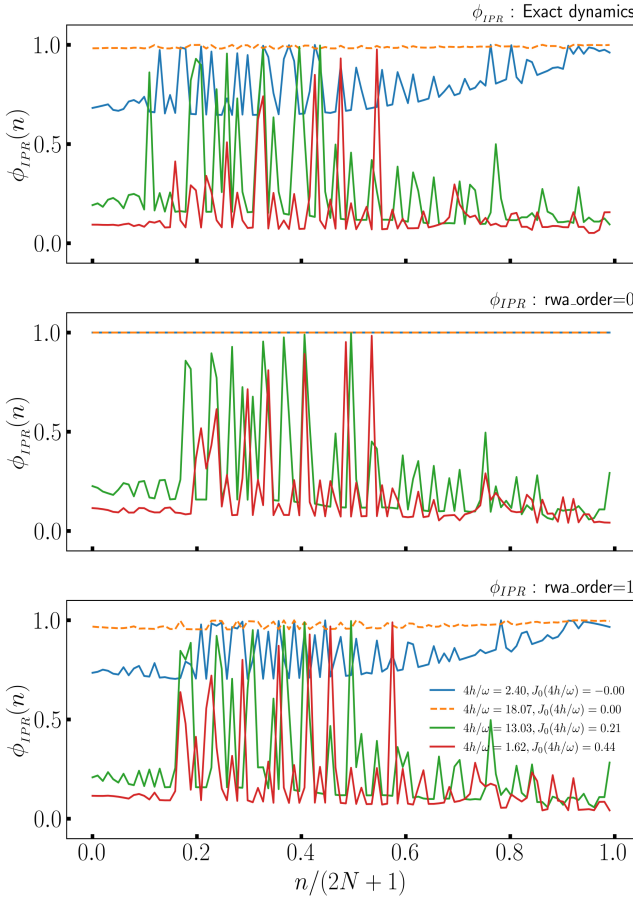


FIG. 5. The comparison between IPR for exact dynamics and RWA with corresponding correction orders. IPR is calculated for four different η 's and corresponding $J_0(\eta) \neq 0$ values. blue: $\eta = 2.40, J_0(\eta) = 0.0$, dashed orange: $\eta = 18.07, J_0(\eta) = 0.0$, green: $\eta = 13.03, J_0(\eta) = 0.21$, red: $\eta = 1.62, J_0(\eta) = 0.44$. IPR plots for RWA with zeroth order aren't enough to describe the exact dynamics, but plots for RWA with first-order correction are similar to the exact dynamics.

IV. THERMALITY TO ATHERMALITY: A PHASE TRANSITION

So far, the dynamics of the Lipkin-Glick-Meshkov model exhibit two distinct scenarios at low and high external drive frequencies; hence, we propose there may be a frequency-induced phase shift. IPR of the floquet modes is computed numerically and plotted in FIG.7 for numerous frequencies in ascending order from frequency $\omega = 1.0$ upto $\omega = 50.0$ so that the system can grow adiabatically, along with the associated drive amplitude h for the first of the localization point, which is $J_0(\frac{4h}{\omega})$. (Top panel) At low-frequency region from $\omega = 1.0$ upto $\omega \sim 9.0$, IPR is lower than unity and it gradually decreased as the system size increases which is $\frac{1}{N}$ variation of IPR which confirms the distribution of participation(Bottom panel). When $N \rightarrow \infty$ IPR appears to

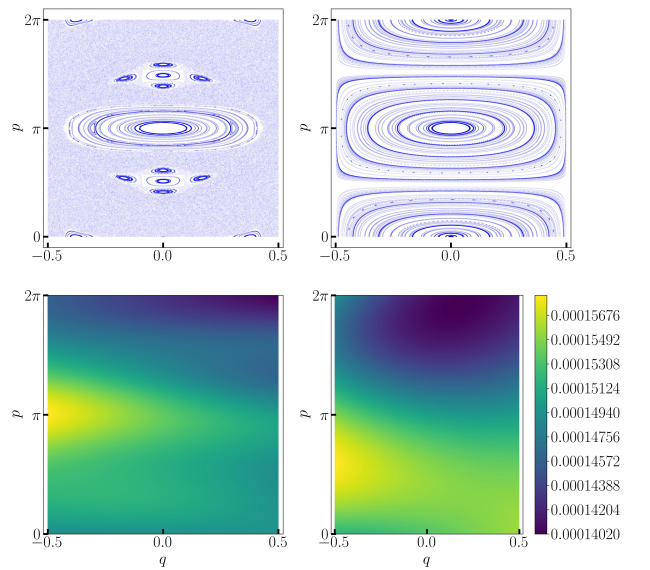


FIG. 6. The above panel describes the phase-space Poincare distribution symmetry breaking smaller drive frequency $\omega = 2.5$ (left) and higher frequency $\omega = 90.0$ (right) for system size $N = 500$ with 100 realisation numbers. At smaller frequencies, the Poincare picture contains chaotic behaviour (top left panel) whereas at the higher frequencies, it is a normal Poincare picture which represents discrete freezing behaviour (top right panel). The bottom panel is Hushimi Q-function average plot for a smaller frequency (bottom left) and has a uniform distribution with less contrast in colour. This means a Q-function distribution in chaotic behaviour. At the right bottom, the Hushimi plot has distinct colour contrast in the Q-function average value which represents a regular dynamics pattern in the system.

be zero which is fully delocalized state. At frequency $\omega \sim 9.0$ there is a sharp rise in IPR plot and IPR remains almost unity (Top panel) for higher frequencies even at change in system sizes. The sudden rise in IPR at frequency confirms phase transition in the frequency domain for LMG long-range spin model.

V. OBSERVATIONS AND DISCUSSION

For ising model quantum many-body localization is present at high drive frequency and corresponding high drive amplitude at localization points obtained by fixing $J_0(2h/\omega) = 0$ for both exact and Rotated wave simulations with fairly weak delocalization away from the localization points. Since the Ising model is integrable, localization can be observed even at tiny ω values, despite the fact that RWA breaks out and analytical approaches beyond the adiabatic limit are complex. In the LMG model, we can see clear localization at localization

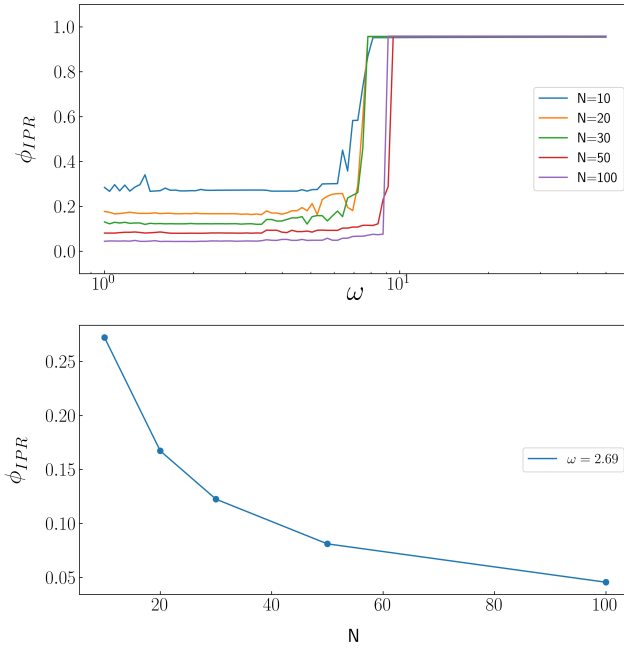


FIG. 7. For different spin sizes, $N = 10, 20, 30, 50, 100$, IPR is plotted at Bessel's first root with first kind $J_0\left(\frac{4h}{\omega}\right)$ varying both the drive amplitude and frequency in LMG spin array. The drive frequency is increased adiabatically from sufficiently low-frequency $O(1)$ and up to high-frequency $O(50)$ for system size $N = 10, 20, 30, 50, 100$ IPR found to be low enough at a small frequency up to a critical frequency where IPR rises to unity abruptly for each system sizes(Top panel). It is also found that at low-frequency regions the system IPR decreases in the scale of N which confirms the distribution of participation of the states of the system (Bottom panel). The change in IPR at critical frequency is sharper as system size increases more, this indicates at infinite large system $N \rightarrow \infty$ the change in IPR to unity is instantaneously resulting in a phase transition at critical frequency.

points, obtained by fixing $J_0(4h/\omega) = 0$, for both the exact and Rotated Wave simulations, with fairly weak delocalization away from those points. Due to the fact that the LMG model is non-integrable and the start of chaos in the thermodynamic limit for small ω is well-known, we can witness near full delocalization in the IPR of the Floquet states for tiny ω .

Consequently, we adiabatically varied ω, h in the LMG model, under the constraint that $\eta = 4h/\omega$ was held at a root of $J_0(\eta)$. There, we observed a crossover or phase change from nearly fully thermal to completely localised behaviour (see FIG.7). Even if the limitation is relaxed, the macroscopic behaviour changes from thermal to athermal. At low frequencies, IPR is observed to decrease with increasing system size N , and when N is big, i.e., $\rightarrow \infty$, IPR appears to evaporate, resulting in a fully thermalized state at $\eta = 4h/\omega$. This is in contrast to the Ising model, which lacks such a transition. Thus, the incorporation of long-range interactions appears to trig-

ger a transition from the thermal phase to the localised phase, a property that will prove useful in the design of MBL engines.

VI. CONCLUSION AND OUTLOOK

As a paradigmatic example, we explored the beginning of Dynamical Many-Body Localization in regularly driven long-range spins for the Lipkin-Glick-Meshkov spin model. The many-body localization is parametrized by the Inverse Participation Ratio of the Floquet eigenstates. We numerically compared the IPR of the LMG model to that of the TFIM for low and high drive frequencies. We also investigated the LMG model's phase space dynamics to analyse the advent of thermal behaviour at low frequencies and localization at high frequencies, as well as the onset of additional approximately conserved quantities in the high-frequency regime for both models.

Conclusion: Long-range spins exhibit strong localization in spin-coordinate space for the LMG model when the drive frequency is $\omega \gg J$, where J represents the spin exchange energy. For the LMG model localization takes place at particular resonances of the drive frequency ω and amplitude h , *i.e.* when $J_0(4h/\omega) = 0$. While similar localization (in momentum space) has been observed for the TFIM case at resonances given by $J_0(2h/\omega) = 0$, the mechanism is different in long-range systems due to the conservation of a different observable (S_x)² in the LMG case, where \mathbf{S} is the total spin. Once the accidental degeneracy is eliminated by a DC transverse field of the form $\sim \hat{S}_x$, the eigenstates can be mapped to a coordinate representation, resulting in robust spatial localization. A strong mobility edge is also seen in the periodically driven LMG model as the frequency is increased adiabatically from $\omega \sim J$ to $\omega \gg J$. In the first regime, the quantum system will thermalize at infinite temperatures because the classical dynamics will have entered a state of dynamical chaos. But in the latter regime, this is perpetually postponed due to dynamical localization. The mobility edge between these regimes shows singular behaviour in the thermodynamic limit, suggesting a quantum phase transition between them. This is not present in the short-range TFIM, where the IPR is too large in the low-frequency limit to induce thermal behaviour. Thus, Floquet engineering in long-range systems is sufficient to induce Thermal and MBL states, and disorder is not required.

Outlook: We have examined a clean system with high symmetry. In all cases, thermalization occurs in addition to integrability-breaking terms (such as disorder), but similar to TFIM, thermalization should be delayed in LMG when at $\omega \gg J$ and $J_0(4h/\omega) = 0$. For systems with Hamiltonian $\mathcal{H} = -\frac{J_{ij}}{|i-j|^\beta} \sum_{ij} \sigma_i^z \sigma_j^z - \sum_i \sigma_i^x$, the less studied intermediate spin-spin interaction power law limits, *i.e.* $0 < \beta < \infty$, rather than the infinite and long-range limit, can be studied further. The adiabatic increase in drive frequency causes a phase transition in

the LMG spin configuration, indicating a future MBL engine with a thermodynamic cycle that operates between the thermal and MBL regimes. There are also opportunities for diabatic corrections.

Acknowledgement: One of the authors (MR) thankfully acknowledges The University of Burdwan for granting the state-funded fellowship.

-
- [1] P. Bordia, H. Lüschen, U. Schneider, M. Knap, and I. Bloch, Periodically driving a many-body localized quantum system, **13**, 460.
- [2] S. Sahoo, I. Schneider, and S. Eggert, Periodically driven many-body systems: A floquet density matrix renormalization group study, .
- [3] A. Das, Exotic freezing of response in a quantum many-body system, **82**, 172402.
- [4] G. B. Mbeng, A. Russomanno, and G. E. Santoro, *The quantum ising chain for beginners*, 2009.09208 [cond-mat, physics:quant-ph].
- [5] H. S. Yamada and K. S. Ikeda, Localization and delocalization properties in quasi-periodically-driven one-dimensional disordered systems, **105**, 054201.
- [6] A. Roy and A. Das, Fate of dynamical many-body localization in the presence of disorder, **91**, 121106 () .
- [7] A. Campa, T. Dauxois, and S. Ruffo, Statistical mechanics and dynamics of solvable models with long-range interactions, **480**, 57.
- [8] T. Eisele and R. S. Ellis, Multiple phase transitions in the generalized curie-weiss model, **52**, 161.
- [9] A. Canning, A class of long range ising spin models described by curie-weiss mean field theory, **185**, 254.
- [10] G. Misguich, V. Pasquier, and J.-M. Luck, Inverse participation ratios in the xxz spin chain, *Phys. Rev. B* **94**, 155110 (2016).
- [11] M. Calixto and E. Romera, Inverse participation ratio and localization in topological insulator phase transitions, **2015**, P06029.
- [12] K. Fujii, Introduction to the rotating wave approximation (RWA): Two coherent oscillations, **8**, 2042.
- [13] J. M. Deutsch, Eigenstate thermalization hypothesis, **81**, 296 () .
- [14] R. Nandkishore and D. A. Huse, Many-body localization and thermalization in quantum statistical mechanics, *Annual Review of Condensed Matter Physics* **6**, 15 (2015), <https://doi.org/10.1146/annurev-conmatphys-031214-014726>.
- [15] M. Srednicki, The approach to thermal equilibrium in quantized chaotic systems, *Journal of Physics A: Mathematical and General* **32**, 1163 (1999).
- [16] M. Rigol and M. Srednicki, Alternatives to eigenstate thermalization, *Physical Review Letters* **108**, 10.1103/physrevlett.108.110601 (2012).
- [17] E. W. Hobson, *On the Second Mean-Value Theorem of the Integral Calculus* (1909).
- [18] J. M. Deutsch, Quantum statistical mechanics in a closed system, **43**, 2046 () .
- [19] M. Srednicki, Chaos and quantum thermalization, **50**, 888.
- [20] L. Reichl, *The Transition to Chaos: Conservative Classical and Quantum Systems*, Fundamental Theories of Physics, Vol. 200 (Springer International Publishing).
- [21] M. Bukov, L. D'Alessio, and A. Polkovnikov, Universal High-Frequency Behavior of Periodically Driven Systems: from Dynamical Stabilization to Floquet Engineering, ArXiv: 1407.4803v2.
- [22] S. Rozhin, Abolfazl, Floquet-induced localization in long-range many-body systems 10.1103/PhysRevResearch.5.013094.
- [23] L. N. Alet Fabien, Many-body localization: An introduction and selected topics 10.1016/j.crhy.2018.03.003.
- [24] S. J. Garratt and S. Roy, Resonant energy scales and local observables in the many-body localized phase, **106**, 054309, publisher: American Physical Society.
- [25] R. B. Stinchcombe, Ising model in a transverse field. i. basic theory, **6**, 2459.
- [26] S. Mukherjee, A. Spracklen, D. Choudhury, N. Goldman, P. Öhberg, E. Andersson, and R. R. Thomson, Modulation-assisted tunneling in laser-fabricated photonic wannier–stark ladders, **17**, 115002, publisher: IOP Publishing.
- [27] S.-H. Lin, B. Sbierski, F. Dorfner, C. Karrasch, and F. Heidrich-Meisner, Many-body localization of spinless fermions with attractive interactions in one dimension, **4**, 002.
- [28] N. C. Murphy, R. Wortis, and W. A. Atkinson, Generalized inverse participation ratio as a possible measure of localization for interacting systems, **83**, 184206, publisher: American Physical Society.
- [29] E. J. Torres-Herrera, I. Vallejo-Fabila, A. J. Martínez-Mendoza, and L. F. Santos, Self-averaging in many-body quantum systems out of equilibrium: Time dependence of distributions, **102**, 062126, publisher: American Physical Society.
- [30] N. Trivedi and D. Heidarian, Can disorder drive a mott insulator into a metal in 2d?, **160**, 296.
- [31] G. Misguich, V. Pasquier, and J.-M. Luck, Inverse participation ratios in the XXZ spin chain, **94**, 155110, publisher: American Physical Society.
- [32] A. Russomanno, R. Fazio, and G. E. Santoro, Thermalization in a periodically driven fully connected quantum ising ferromagnet, **110**, 37005.
- [33] T. Mori, Prethermalization in the transverse-field ising chain with long-range interactions, **52**, 054001, publisher: IOP Publishing.
- [34] F. E. H. George Arfken, Hans Weber, *Mathematical Methods for Physicists*.
- [35] B. Sciolla and G. Birolì, Quantum quenches and off-equilibrium dynamical transition in the infinite-dimensional bose-hubbard model, **105**, 220401.
- [36] R. A. Kidd, M. K. Olsen, and J. F. Corney, Quantum chaos in a bose-hubbard dimer with modulated tunneling, *Phys. Rev. A* **100**, 013625 (2019).
- [37] A. Roy and A. Das, Fate of dynamical many-body localization in the presence of disorder, **91**, 121106 () .
- [38] N. Srivatsa, R. Moessner, and A. E. Nielsen, Many-body delocalization via emergent symmetry, **125**, 240401.
- [39] *Quantum ising phase transition*.
- [40] B. Marcos, A. Gabrielli, and M. Joyce, Relaxation of

- quasi-stationary states in long range interacting systems and a classification of the range of pair interactions, [10, 676](#).
- [41] A. Haldar and A. Das, Dynamical many-body localization and delocalization in periodically driven closed quantum systems, [529, 1600333](#).
- [42] N. Yunger Halpern, C. D. White, S. Gopalakrishnan, and G. Refael, Quantum engine based on many-body localization, [99, 024203](#).